ACS NANO
Cite This: ACS Nano 2017, 11, 10230-10235
www.acsnano.org

ARTICLE

Highly Deformable Origami Paper Photodetector Arrays

Chun-Ho Lin,[†] Dung-Sheng Tsai,[†] Tzu-Chiao Wei,[†] Der-Hsien Lien,[†] Jr-Jian Ke,[†] Chun-Hao Su,[‡] Ju-Yen Sun,[‡] Ying-Chih Liao,[‡] and Jr-Hau He*[,†]

[†]Computer, Electrical, and Mathematical Sciences and Engineering (CEMSE) Division, King Abdullah University of Science & Technology (KAUST), Thuwal 23955-6900, Saudi Arabia

[‡]Department of Chemical Engineering, National Taiwan University, Taipei 106, Taiwan

Supporting Information

ABSTRACT: **Flexible electronics will form the basis of many next-generation technologies, such as wearable devices, biomedical sensors, the Internet of things, and more. However, most flexible devices can bear strains of less than 300% as a result of stretching. In this work, we demonstrate a simple and low-cost paper-based photodetector array featuring superior deformability using printable ZnO nanowires, carbon electrodes, and origami-based techniques. With a folded Miura structure, the paper photodetector array can be oriented in four different directions *via* tessellated parallelograms to provide the device with excellent omnidirectional light harvesting capabilities. Additionally, we demonstrate that the device can be repeatedly stretched (up to 1000% strain), bent (bending angle ±30°), and twisted (up to 360°) without degrading performance as a result of the paper folding technique, which enables the ZnO nanowire layers to remain rigid even as the device is deformed. The origami-based strategy described herein suggests avenues for the development of next-generation deformable optoelectronic applications.**

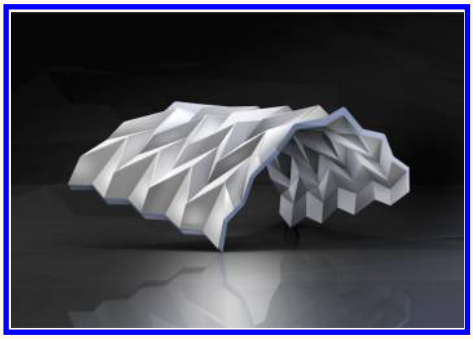

KEYWORDS: *origami, printing technology, paper device, flexible electronic, deformable optoelectronic*

The promise of flexible and stretchable electronics suggests an exciting future beyond traditional rigid wafer and printed circuit board technologies. With the capacity to integrate with soft materials and curvilinear surfaces, such flexible devices will enable a variety of applications, including biomedical sensors,[1] home healthcare,[2] wearable technology,[3] electronic skins,[4] mobile devices,[5] the Internet of things,[6] and more.[7] Over the past few years, researchers have explored a wide variety of deformable devices using various soft materials[6,8−11] and different structures, such as island bridges,[12] open mesh geometries,[9,13] and wave-like configurations.[14]

Paper, a soft material that is truly low cost (one tenth the price of plastic films and one percent as much as silicon),[15] is lightweight, flexible, biodegradable, and recyclable.[16] Additionally, with the use of proper additives and manufacturing processes, it is possible to engineer paper with a large range of properties, including hydrophilicity or hydrophobicity, porous or watertight structures, opacity or near transparency, weak or strong mechanical properties, and surfaces that are coarse or as smooth as glass.[16,17] To date, researchers have explored many paper-based electronic devices, such as transistors,[18] solar cells,[19] light emission diodes,[20] radio frequency identification tags,[21] electronic memory devices,[15,22] and light sensors,[23] using low-cost fabrication processes (*e.g.*, spin coating, screen- and inkjet-printing, and sputtering).[18,19,24] However, the stretchability of paper-based devices is limited (less than 5%),[25] thus hindering applications in flexible electronics.

Origami is the ancient art of paper folding, once limited to art circles, but now becoming of greater interest to science and technology due to the technique's ability to adopt a variety of shapes and structures while also making the material easier to stretch and compress. Utilizing such folding techniques has enabled scientists to develop exciting technologies at both the macroscale and microscale, including space-saving rocketry,[26] a foldable lithium ion battery,[27] a nanopaper antenna,[28] and DNA nanorobots for drug delivery.[29]

In this work, we combined similar folding concepts with a paper-based electronic device to achieve a 1000% stretchable origami paper photodetector array (OPPDA). We fabricated this device by screen-printing ZnO nanowires and carbon electrodes on common office printing paper and then utilizing the Miura origami folding method[30,31] to produce a structure that can expand and collapse with an accordion-like motion while maintaining reliable photosensing performance (photo-to-dark current ratio (PDCR) > 5) in the detection of ultraviolet (UV) light even under extreme deformation. This

Received: July 9, 2017
Accepted: September 25, 2017
Published: September 25, 2017

DOI: 10.1021/acsnano.7b04804
ACS Nano 2017, 11, 10230−10235

stability is made possible due to the nature of the Miura structure, which consists of tessellated parallelograms. The parallelogram faces are divided by four-coordinated origami creases—three mountain folds and one valley fold[32]—that join together at a vertex. This Miura folding structure orients the individual ZnO photodetectors (PDs) on the parallelogram faces in four different directions, thus providing the OPPDA with exceptional omnidirectional photodetection in a manner that cannot be easily achieved using conventional rigid substrates.

Moreover, the Miura fold utilizes a special origami technique called "rigid origami" (*i.e.*, treating the folds as hinges that join two flat and rigid surfaces),[33] which allows the parallelogram faces to remain rigid as the overall device is deformed. As a result, during deformation there are no tensile forces acting on the ZnO active materials printed on the parallelogram faces, something that is impossible for conventional flexible electronics to achieve on soft substrates. Maintaining the structural rigidity of the ZnO PDs enables the OPPDA to maintain its ultrastable performance even after experiencing 400 cycles of sequential stretching, bending, and twisting. This origami paper-based strategy demonstrates an alternative paradigm for the development of next-generation deformable optoelectronic applications in sensing, imaging, and intrachip optical interconnects.[34]

RESULTS AND DISCUSSION

Structural and Photosensing Characteristics of the Miura-Folded OPPDA. To form the array of PDs, we screen-printed photoactive ZnO nanowires that were connected in series-parallel using carbon electrodes on an 11 cm × 11 cm piece of printer paper (see Methods for more details). Using this substrate, we then made the necessary folds[31] to generate the Miura origami structure that made up the ultrastretchable and flexible OPPDA device. Figure 1a is the schematic of the

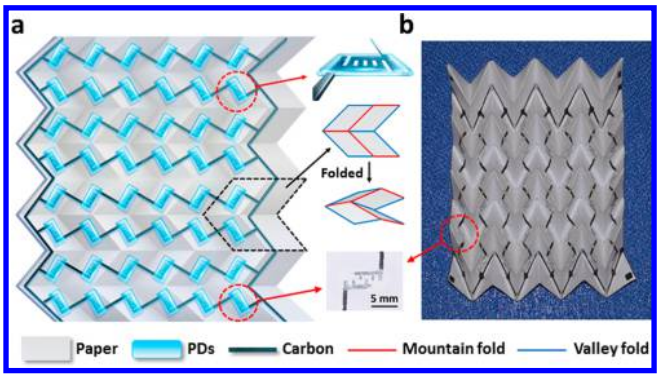

Figure 1. Architecture of the Miura OPPDA. (a) Schematic diagram of the OPPDA in the completely unfolded state. The first inset on the top right shows the 3D structure of a PD unit cell. The second inset in the middle demonstrates a period cell consisting of four parallelograms of the Miura origami and its folded state. The last inset on the bottom is a photograph of a real PD unit cell. (b) Photographic image of the device.

OPPDA in a completely unfolded state, consisting of individual parallelogram faces that are formed from the combination of the mountain and valley paper folds. The ZnO PD unit cells are centered on each parallelogram.

One of the advantages of the Miura folding technique is that it can take a flat surface and compress it into a very small volume. In this case, we were able to collapse the structure so it was just 1 cm × 11 cm in area, as well as expand it again into the original sized sheet of paper. Furthermore, the Miura OPPDA can also be rapidly opened and closed in just one motion by either pushing or pulling on the opposite ends of the folded paper. Thus, with this origami technique, we were able to transform the device from a 2D sheet to a three-dimensional (3D) structure, in which the many identical parallelogram faces could fold together to form 3D pyramids (Figure 1b). Note that the parallelograms do not themselves deform during this transition because the process of folding and unfolding takes place along the paper creases that outline each face. This enables the photoactive materials to remain in a flat, rigid configuration even as the full device is bent and stretched.

The OPPDA is made of many individual ZnO PDs, and the structural and photosensing characteristics of one are shown in Figure S1 of the Supporting Information. In order to demonstrate the UV sensitivity of the overall OPPDA, we measured the current−voltage (I−V) curves of the device in the dark and under UV illumination (Figure 2a). In this work, the

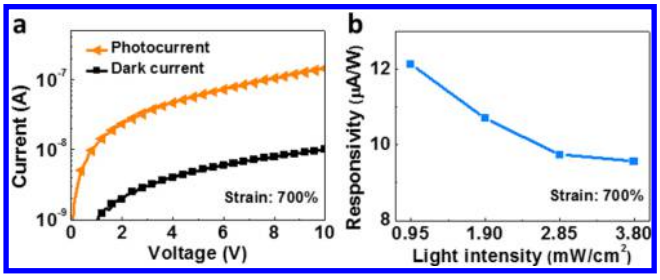

Figure 2. Photosensing performance of the OPPDA. (a) I−V curves of the OPPDA measured in the dark and under UV illumination. (b) Responsivity of the OPPDA as a function of UV light intensity and 700% strain.

typical measurement conditions were under UV illumination with an intensity of 3.8 mW/cm^2 at room temperature at 10 V bias unless otherwise noted. The photocurrent of the OPPDA was approximately 1 order of magnitude larger than the dark current (PDCR = 13.4). Moreover, as shown in Figure 2b, the responsivity of the OPPDA decreased as the light intensity was increased from 0.95 mW/cm^2 to 3.8 mW/cm^2. A possible reason for this trend is that an excess number of charge carriers under high-intensity illumination may increase the carrier recombination rate,[35−37] leading to the reduction of responsivity. Thus, with the integration of the origami structure and the printed array of PDs, the OPPDA demonstrates reliable detection of UV light at a range of intensities.

Noise-equivalent power (NEP) is an important parameter to determine the sensitivity of PDs and defined as the required optical power to give a signal-to-noise ratio of 1 with a bandwidth of 1 Hz. On the other hand, the detectivity (D^*), the reciprocal of NEP, is usually used to evaluate the performance of PDs. In this study, the NEP of the OPPDA under a 10 V bias is 1.23×10^{-9} W/cm Hz$^{1/2}$ calculated by $\mathrm{NEP} = P/f^{1/2} = (2eJ_d)^{1/2}/R_I$, where P is the incident power, f is the frequency bandwidth of PDs, e is charge of an electron, J_d is the dark current density, and R_I is responsivity, resulting in a D^* value of 8.14×10^8 cm Hz$^{1/2}$/W. To further improve the detectivity of the OPPDA, an advanced fabrication method such as the inkjet printing can be used to fabricate high-quality ZnO layers,[38] for enhancing the responsivity and detectivity of the OPPDA.

DOI: 10.1021/acsnano.7b04804
ACS Nano 2017, 11, 10230−10235

Ultrahigh Deformation and Stable Operation of the OPPDA. To highlight the excellent and stable UV light detection of the flexible and stretchable OPPDA, we measured the device's light-sensing capabilities as it was being stretched, bent, and twisted. First, we standardized the way we defined the OPPDA's strain (*i.e.*, stretching state) as $[(L_x - l_{x0})/l_{x0}] \times 100\%$ using the dimensions of the device in the x direction as shown in Figure 3a, in which L_x is the dimension of the

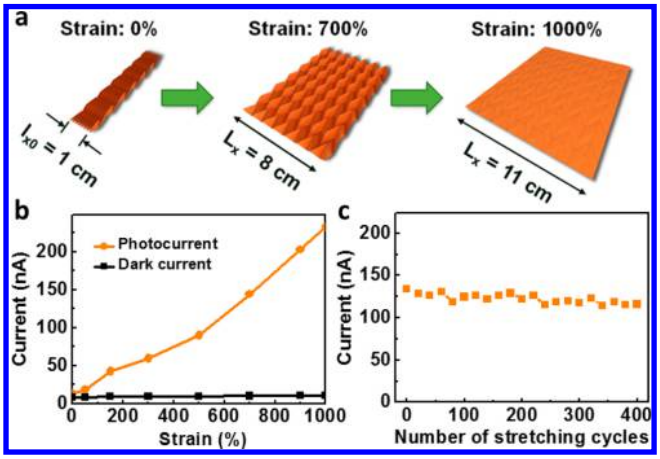

Figure 3. Illustration of the OPPDA under different strain states and photosensing measurements of the stretched OPPDA. (a) Schematic diagram of the OPPDA under strains of 0%, 700%, and 1000% and the respective folding states of the device. (b) The dark current and photocurrent of the OPPDA were measured as a function of strain under dark and UV-illuminated conditions. (c) Photocurrent of the OPPDA as a function of stretching cycles measured under UV illumination.

unfolded state and l_{x0} is the dimension of the completely compressed state (l_{x0} = 1 cm). The strain increases as the paper is transitioned from the folded to unfolded state. For example, the strain is 0% for L_x = 1 cm (the extreme folded state), 700% for L_x = 8 cm (the typical resting state of the Miura folding pattern, revealing the 3D pyramidal structures), and 1000% for L_x = 11 cm (the totally unfolded state of the flat sheet of paper).

In Figure 3b, we measured the dark current and photocurrent of the OPPDA as a function of strain. From the folded to unfolded states, the photocurrent increased with strain due to the more effective areal-density absorption of UV light by the PD unit cells as the OPPDA was transformed from its 3D to 2D configurations under normal incident light illumination. During this physical transition, the dark current remained stable and showed no noticeable change even under high stain. In addition, under a strain of up to 1000% and after 400 continuous stretching cycles (a stretching cycle began at 700% strain, increased to 1000%, then decreased to 0%, before returning back to 700%), the photocurrent variation was ultralow (Figure 3c), indicating the robustness of the flexible and stretchable device. We attribute this stable photosensing performance to the rigid origami technique and the excellent bonding between the printed carbon electrodes and PDs on the paper substrate. Thus, by incorporating the array of PDs with the Miura origami paper design, we were able to create a device that offers fully reversible compressibility/stretchability without creating substantial strain in the PD materials themselves that would otherwise hurt the photosensing performance.

In addition to ultrahigh stretchability, we also measured the performance of the OPPDA as it was being bent and twisted. Figure 4a illustrates the bending angle of the device,

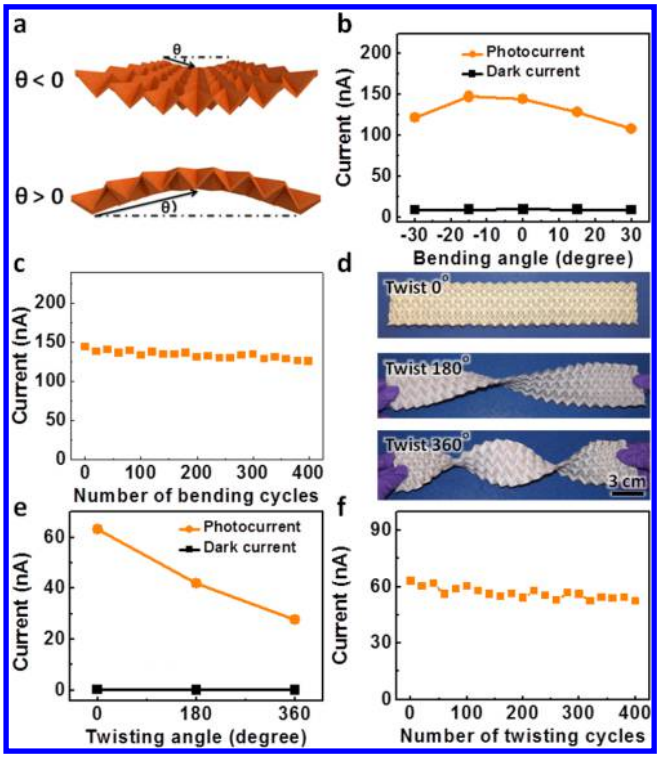

Figure 4. OPPDA photosensing under bending and twisting conditions. (a) Schematic illustration of the OPPDA in a concave (bending angle θ < 0°) and convex (bending angle θ > 0°) bending configuration. (b) Bending-angle-dependent photocurrent and dark current of the device under 700% strain. (c) Photocurrent *versus* bending cycles under UV illumination. (d) Optical photograph of the OPPDA subjected to torsion (angle of twist = 0°, 180°, and 360°). (e) Dark current and photocurrent of the OPPDA *versus* twist angle measured in the dark and under UV illumination. (f) Photocurrent as a function of the number of twist cycles under UV illumination.

demonstrating the concave (bending angle θ < 0°) and convex (bending angle θ > 0°) configurations in the upper and lower images, respectively. Under these conditions, we measured the bending-angle-dependent photocurrent and dark current of the device at 700% strain (Figure 4b). The OPPDA exhibited a dark current as low as 9 nA and a PDCR that ranged from 11 to 13 for the bending conditions of $-30° \leq \theta \leq 30°$, as good as the device performance under the undeformed state. Figure 4c shows the device photocurrent for up to 400 bending cycles (a bending cycle started at θ = 0°, increased to 30°, then lowered to −30°, before returning back to 0°), demonstrating the excellent endurance of the device as it retained the same level of photosensing capability throughout the test.

Twisting is another type of mechanical deformation that is important for flexible electronics to possess. Figure 4d is a photograph of the OPPDA as it is being subjected to torsion (the angle of twist = 0°, 180°, and 360°). We measured the dark current and photocurrent of the device as a function of its twisting angle (Figure 4e), and the results showed that the OPPDA maintained a low dark current (<10 nA) even under significant torsion (360°). As the twisting angle increases, the device also becomes increasingly illuminated from its back side

DOI: 10.1021/acsnano.7b04804
ACS Nano 2017, 11, 10230−10235

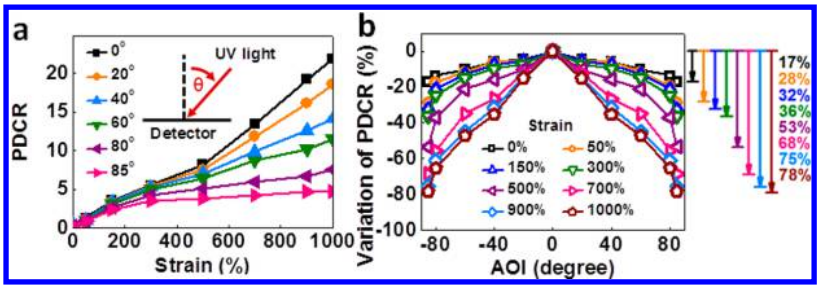

Figure 5. AOI-dependent photosensing of the OPPDA. (a) The PDCR of the OPPDA was measured as a function of strain at different AOIs of UV light. (b) AOI-dependent variation of the device's PDCR for different amounts of strain applied. The far-right arrows indicate the decreasing ratio of PDCR from an AOI of 0° to 85° for different strain conditions.

(*i.e.*, the opposite side on which the array of PDs were printed), and therefore the photocurrent expectedly decreases as the light must pass through the paper to reach the detectors. As shown in Figure S2, compared to front-side UV illumination, the photocurrent of the device decreases by up to 1 order of magnitude under back-side UV illumination. Figure 4f displays the twisting endurance test for the OPPDA, demonstrating that there was no significant change in the device's photocurrent at the 0° condition before and after 400 cycles of twisting (a cycle began at a twisting angle of 0°, increased to 360°, then returned back 0°). At the end of the sequential mechanical tests (400 cycles stretching, 400 cycles bending, and 400 cycles twisting), we observed no voids, cracks, or delamination in the carbon electrodes at the folded creases of the device (Figure S3), thus demonstrating the robustness of the origami paper-based design.

Furthermore, to study the omnidirectionality of the device, we measured the PDCR of the OPPDA as a function of strain at different angles of incidence (AOI), as shown in Figure 5a. Under high strain (~1000%), the PDCR value decreased with AOI due to the high reflection of light on the nearly planar surface[39] (*i.e.*, the totally unfolded state). In contrast, under low strain (<500%), the PDCR value changed very little (<5) at AOIs from 0° to 85°, indicating the OPPDA exhibits excellent omnidirectional light detection when it is in its folded configuration. In order to further assess the omnidirectional photodetection capabilities of the OPPDA, we defined the AOI-dependent variation of PDCR as $[(PDCR_\theta - PDCR_0)/PDCR_0] \times 100\%$, in which $PDCR_\theta$ is the PDCR value at an incident angle of θ, and $PDCR_0$ is the PDCR value at normal incidence.[40] As shown in Figure 5b, the AOI-dependent variation of PDCR under low strain (between 0% and 500%) is very small (between −20% and −40%) as the AOI varies from 0° to 85°, in contrast to when the device is under high strain (>500%). These omnidirectional measurements demonstrate the reliability of the device to detect UV light at a wide range of detection angles (170° total), which is a key feature desired in flexible optoelectronics.

To further study the topographical adaptability of the OPPDA, we performed four sets of real-world demonstrations. In Figure 6a,b, we measured the dark current and photocurrent of the device with and without UV illumination after mounting the device against the inside of a fish bowl and on the surface of a human arm. In these two situations, the PDCR values for the fish bowl and arm were up to 7.5 and 5.2, respectively, indicating outstanding photodetection even under situations featuring ultrahigh tension, flexure, and torsion. The other two applications involved mounting the OPPDA on a basketball and a set of stairs, which are shown in Figure S4, demonstrating

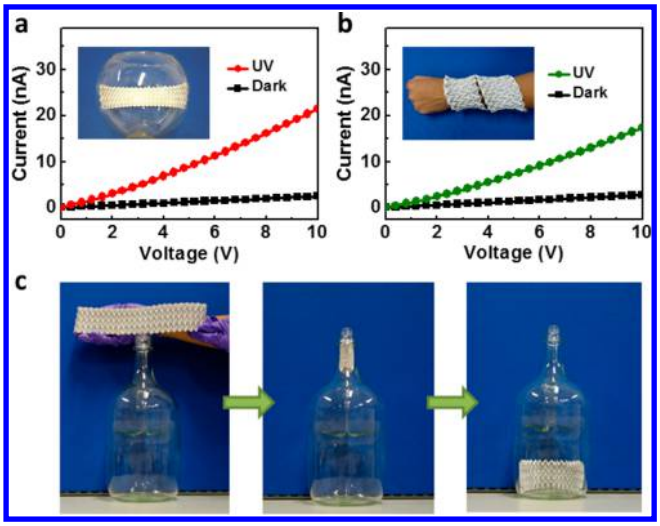

Figure 6. Real-world applications of the OPPDA to demonstrate the device's deformability and topographical adaptability. *I*–*V* curves of the OPPDA device mounted (a) in a fish bowl and (b) on a person's arm, as measured in the dark and under UV illumination. (c) Images of the device passing through the narrow mouth of a glass bottle.

PDCR values of up to 16 and 14.7, respectively. Overall, in these four real-world demonstrations, the photocurrent of the OPPDA was approximately 1 order of magnitude larger than the dark current, confirming the high topographical adaptability of the device. To further highlight the deformability of the OPPDA, Figure 6c demonstrates how the device can be folded into a compact shape that can easily pass through the narrow mouth of a glass bottle. This ability to compress into a very small volume is particularly distinct to the OPPDA, as such deformation is not possible for conventional flexible electronics.

CONCLUSION

In summary, the strategies presented herein demonstrate the degree to which highly deformable properties, including stretching (up to 1000% strain), bending (±30°), and twisting (up to 360°) can be achieved in conjunction with high-performance photodetection through the integration of Miura origami, array design, and paper printing processes, even while using intrinsically brittle but high-performing inorganic electronic/optical materials. In addition, the device features exceptional omnidirectional detection capabilities by facing the PDs in four different directions on the angled tessellated parallelograms of the Miura folding structure. Furthermore, after 400 sequential cycles of tension, bending, and twisting

DOI: 10.1021/acsnano.7b04804
ACS Nano 2017, 11, 10230–10235

tests, the OPPDA continued to demonstrate a stable photoresponse.

With the use of origami, we can improve the potential application and characteristics of paper-based devices. However, this origami-based concept is not limited to just paper electronics, but could also be used for other devices that feature hard materials in order to make it possible for them to be stretched or folded. We believe this highly deformable electronics design featuring the Miura origami structure demonstrates a promising direction for future developments in flexible electronics.

METHODS

Fabrication of the OPPDA. To prepare the devices, we first screen-printed a carbon paste (C1399, Advanced Electronic Materials Inc.) onto printer paper (80 gsm, Double A) and then baked the material at 70 °C in a vacuum oven for 20 min to remove organic solvent residues. ZnO nanowires were prepared *via* the vapor−liquid−solid method[41] by heating a mixture of 6.6 g of ZnO (Sigma-Aldrich, ≥99.0%) and 3.3 g of carbon powder (Sigma-Aldrich, 99.95%) in a tube furnace (O1200-60IT, NBD Tech.) at 930 °C and 1 atm pressure with 200 sccm Ar gas flow. A silicon chip cleaned by acetone (Fisher Scientific) and deionized water was placed in the downwind position of the reactants. The ZnO nanowires that formed on the silicon chip were then scraped and collected using a laboratory spatula. We then made a ZnO nanowire ink using a sol−gel method[42] from a mixture of 1 g of ZnO nanowires, 5 mL of ethanol (Sigma-Aldrich, ≥99.8%), and 50 μL of surfactant (Triton X-100, Fisher Scientific). The ZnO ink was screen-printed across the carbon electrodes to form 30 μm thick photoactive ZnO nanowire layers (Figure S1), and then we placed the device on a hot plate for 10 min to remove the ethanol. Finally, the paper substrate with the patterned array of PDs was folded into a Miura-origami structure. We reinforced the carbon electrodes on the fold lines with silver paste (Sigma-Aldrich, 50−60 wt %).

***I*−*V* Characterization of the OPPDA.** A Keithley 2400-SCS semiconductor characterization system was used to measure the *I*−*V* characteristics of the OPPDA devices under various conditions, including different intensities of light, AOIs, and various curved and uneven surfaces at room temperature. An ozone-generating UV lamp (Spectroline Co., XX-15G) that emitted light at 185 and 254 nm wavelengths was used to perform the measurements (the UV irradiance intensity at 254 nm is almost 10 times larger than that at 185 nm).[43] Unless otherwise noted, the samples were characterized under conditions featuring a light intensity of 3.8 mW/cm^2 at 10 V bias.

We used an OPPDA device that was 11 cm × 11 cm in size (shown in Figure 1b) to execute the basic photosensing (Figure 2b,c), stretching (Figure 3a,b), omnidirectional (Figure 4a,b), and bending measurements (Figure 5b,c). To better demonstrate the OPPDA's twisting properties and topographical adaptability, a larger device featuring a size of 8 cm × 32 cm was used to perform the twisting measurements (Figure 5e,f) and to demonstrate the four real-world applications (Figure 6a,b and Figure S4a,b). All the measurements were performed at least 5 times, except the stretching, bending, and twisting endurance tests, in which we collected a data point after every 20 cycles (the device was held for 1 s at each state during these tests).

We calculated PDCR using eq 1:[44]

$$\mathrm{PDCR} = (I_{ph} - I_d)/I_d \quad (1)$$

in which I_d is the dark current and I_{ph} is the photocurrent under UV illumination.

Responsivity (R_I) was calculated using eq 2:[45]

$$R_I = I_p/(P_{in} \times A) \quad (2)$$

in which I_p is the total generated photocurrent of the whole device, P_{in} is the incident UV light intensity, and A is the active area of the device (the ZnO flim area).

ASSOCIATED CONTENT

Supporting Information

The Supporting Information is available free of charge on the ACS Publications website at DOI: 10.1021/acsnano.7b04804.

The structure and sensing performance of a single ZnO nanowire PD unit cell, the OPPDA's photosensing ability for front-side and back-side UV illumination, a comparison of the cross-sectional SEM images before and after the stretching, bending, and twisting tests demonstrating the mechanical robustness of the carbon electrodes, two real-world applications for the OPPDA to demonstrate its topographical adaptability, and the time response of the OPPDA device (PDF)

AUTHOR INFORMATION

Corresponding Author

*E-mail: jrhau.he@kaust.edu.sa.

ORCID

Der-Hsien Lien: 0000-0001-6774-2074

Ying-Chih Liao: 0000-0001-9496-4190

Jr-Hau He: 0000-0003-1886-9241

Notes

The authors declare no competing financial interest.

ACKNOWLEDGMENTS

This work was financially supported by the King Abdullah University of Science and Technology (KAUST) Office of Sponsored Research (OSR) (OSR-2016-CRG5-3005), KAUST solar center (FCC/1/3079-08-01), and KAUST baseline funding.

REFERENCES

(1) Rogers, J. A.; Someya, T.; Huang, Y. G. Materials and Mechanics for Stretchable Electronics. *Science* **2010**, *327*, 1603−1607.

(2) Axisa, F.; Schmitt, P. M.; Gehin, C.; Delhomme, G.; McAdams, E.; Dittmar, A. Flexible Technologies and Smart Clothing for Citizen Medicine, Home Healthcare, and Disease Prevention. *IEEE Trans. Inf. Technol. Biomed.* **2005**, *9*, 325−336.

(3) Kim, D. H.; Xiao, J. L.; Song, J. H.; Huang, Y. G.; Rogers, J. A. Stretchable, Curvilinear Electronics Based on Inorganic Materials. *Adv. Mater.* **2010**, *22*, 2108−2124.

(4) Kim, D. H.; Ahn, J. H.; Choi, W. M.; Kim, H. S.; Kim, T. H.; Song, J.; Huang, Y. Y.; Liu, Z.; Lu, C.; Rogers, J. A. Stretchable and Foldable Silicon Integrated Circuits. *Science* **2008**, *320*, 507−511.

(5) Pryss, R.; Tiedeken, J.; Kreher, U.; Reichert, M. Towards Flexible Process Support on Mobile Devices. In *Forum at the Conference on Advanced Information Systems Engineering*; Springer: Berlin, Heidelberg, 2010; pp 150−165.

(6) Zhan, Y.; Mei, Y.; Zheng, L. Materials Capability and Device Performance in Flexible Electronics for the Internet of Things. *J. Mater. Chem. C* **2014**, *2*, 1220−1232.

(7) Blees, M. K.; Barnard, A. W.; Rose, P. A.; Roberts, S. P.; McGill, K. L.; Huang, P. Y.; Ruyack, A. R.; Kevek, J. W.; Kobrin, B.; Muller, D. A.; McEuen, P. L. Graphene Kirigami. *Nature* **2015**, *524*, 204−207.

(8) Wang, S.; Weil, B. D.; Li, Y.; Wang, K. X.; Garnett, E.; Fan, S.; Cui, Y. Large-Area Free-Standing Ultrathin Single-Crystal Silicon as Processable Materials. *Nano Lett.* **2013**, *13*, 4393−4398.

(9) Kim, D. H.; Song, J.; Choi, W. M.; Kim, H. S.; Kim, R. H.; Liu, Z.; Huang, Y. Y.; Hwang, K. C.; Zhang, Y. W.; Rogers, J. A. Materials and Noncoplanar Mesh Designs for Integrated Circuits with Linear Elastic Responses to Extreme Mechanical Deformations. *Proc. Natl. Acad. Sci. U. S. A.* **2008**, *105*, 18675−18680.

(10) Yan, C.; Cho, J. H.; Ahn, J. H. Graphene-Based Flexible and Stretchable Thin Film Transistors. *Nanoscale* **2012**, *4*, 4870−4882.

DOI: 10.1021/acsnano.7b04804
ACS Nano 2017, 11, 10230−10235

(11) Pu, J.; Li, L. J.; Takenobu, T. Flexible and Stretchable Thin-Film Transistors Based on Molybdenum Disulphide. *Phys. Chem. Chem. Phys.* **2014**, *16*, 14996−15006.
(12) Li, R.; Li, M.; Su, Y. W.; Song, J. H.; Ni, X. Q. An Analytical Mechanics Model for the Island-Bridge Structure of Stretchable Electronics. *Soft Matter* **2013**, *9*, 8476−8482.
(13) Hung, P. J.; Jeong, K.; Liu, G. L.; Lee, L. P. Microfabricated Suspensions for Electrical Connections on the Tunable Elastomer Membrane. *Appl. Phys. Lett.* **2004**, *85*, 6051−6053.
(14) Choi, W. M.; Song, J.; Khang, D. Y.; Jiang, H.; Huang, Y. Y.; Rogers, J. A. Biaxially Stretchable "Wavy" Silicon Nanomembranes. *Nano Lett.* **2007**, *7*, 1655−1663.
(15) Lien, D. H.; Kao, Z. K.; Huang, T. H.; Liao, Y. C.; Lee, S. C.; He, J. H. All-Printed Paper Memory. *ACS Nano* **2014**, *8*, 7613−7619.
(16) Russo, A.; Ahn, B. Y.; Adams, J. J.; Duoss, E. B.; Bernhard, J. T.; Lewis, J. A. Pen-on-Paper Flexible Electronics. *Adv. Mater.* **2011**, *23*, 3426−3430.
(17) Tobjörk, D.; Österbacka, R. Paper Electronics. *Adv. Mater.* **2011**, *23*, 1935−1961.
(18) Kim, Y. H.; Moon, D. G.; Han, J. I. Organic TFT Array on a Paper Substrate. *IEEE Electron Device Lett.* **2004**, *25*, 702−704.
(19) Leonat, L.; White, M. S.; Głowacki, E. D.; Scharber, M. C.; Zillger, T.; Rühling, J.; Hübler, A.; Sariciftci, N. S. 4% Efficient Polymer Solar Cells on Paper Substrates. *J. Phys. Chem. C* **2014**, *118*, 16813−16817.
(20) Kim, J. Y.; Park, S. H.; Jeong, T.; Bae, M. J.; Song, S.; Lee, J.; Han, I. T.; Jung, D.; Yu, S. Paper as a Substrate for Inorganic Powder Electroluminescence Devices. *IEEE Trans. Electron Devices* **2010**, *57*, 1470−1474.
(21) Yang, L.; Rida, A.; Vyas, R.; Tentzeris, M. M. RFID Tag and RF Structures on a Paper Substrate Using Inkjet-Printing Technology. *IEEE Trans. Microwave Theory Tech.* **2007**, *55*, 2894−2901.
(22) Martins, R.; Barquinha, P.; Pereira, L.; Correia, N.; Gonçalves, G.; Fortunato, I. F. E. Write-Erase and Read Paper Memory Transistor. *Appl. Phys. Lett.* **2008**, *93*, 203501.
(23) Aga, R. S.; Lombardi, J. P.; Bartsch, C. M.; Heckman, E. M. Performance of a Printed Photodetector on a Paper Substrate. *IEEE Photonics Technol. Lett.* **2014**, *26*, 305−308.
(24) Lim, W.; Douglas, E. A.; Norton, D. P.; Pearton, S. J.; Ren, F.; Heo, Y. W.; Son, S. Y.; Yuh, J. H. Low-Voltage Indium Gallium Zinc Oxide Thin Film Transistors on Paper Substrates. *Appl. Phys. Lett.* **2010**, *96*, 053510.
(25) Maraisa, A.; Utsela, S.; Gustafssonb, E.; Wågberg, L. Towards a Super-Strainable Paper Using the Layer-by-Layer Technique. *Carbohydr. Polym.* **2014**, *100*, 218−224.
(26) Nishiyama, Y. Miura Folding: Applying Origami to Space Exploration. *Int. J. Pure Appl. Math.* **2012**, *79*, 269−279.
(27) Cheng, Q.; Song, Z.; Ma, T.; Smith, B. B.; Tang, R.; Yu, H.; Jiang, H.; Chan, C. K. Folding Paper-Based Lithium-Ion Batteries for Higher Areal Energy Densities. *Nano Lett.* **2013**, *13*, 4969−4974.
(28) Nogi, M.; Komoda, N.; Otsuka, K.; Suganuma, K. Foldable Nanopaper Antennas for Origami Electronics. *Nanoscale* **2013**, *5*, 4395−4399.
(29) Douglas, S. M.; Bachelet, I.; Church, G. M. A Logic-Gated Nanorobot for Targeted Transport of Molecular Payloads. *Science* **2012**, *335*, 831−834.
(30) Schenk, M.; Guest, S. D. Geometry of Miura-Folded Metamaterials. *Proc. Natl. Acad. Sci. U. S. A.* **2013**, *110*, 3276−3281.
(31) Schroder, D. K. *Semiconductor Material and Device Characterization*; John Wiley & Sons, 2006.
(32) Buri, H.; Weinand, Y. Origami−Folded Plate Structures, Architecture. In *10th World Conference on Timber Engineering*; 2008; pp 2−5.
(33) M, S.; D, G. S. Origami Folding: a Structural Engineering Approach. In *Origami 5: Fifth International Meeting of Origami Science, Mathematics, and Education*; CRC Press: Boca Raton, FL, 2011; pp 291−303.
(34) Chang, M. F.; Roychowdhury, V. P.; Zhang, L.; Shin, H.; Qian, Y. RF/Wireless Interconnect for Inter- and Intra-Chip Communications. *Proc. IEEE* **2001**, *89*, 456−466.
(35) Mehta, R. R.; Sharma, V. S. Photoconductive Gain Greater than Unity in CdSe Films with Schottky Barriers at Contacts. *J. Appl. Phys.* **1973**, *44*, 325−328.
(36) Saleh, B. E.; Teich, M. C. *Fundamentals of Photonics*; Wiley: New York, 1991.
(37) Chen, M. W.; Retamal, J. R. D.; Chen, C. Y.; He, J. H. Photocarrier Relaxation Behavior of a Single ZnO Nanowire UV Photodetector: Effect of Surface Band Bending. *IEEE Electron Device Lett.* **2012**, *33*, 411−413.
(38) Feng, Z. C. *Handbook of Zinc Oxide and Related Materials: Vol. Two, Devices and Nano-Engineering*; CRC Press, 2012.
(39) Greenler, R. G. Infrared Study of Adsorbed Molecules on Metal Surfaces by Reflection Techniques. *J. Chem. Phys.* **1966**, *44*, 310−315.
(40) Wei, W. R.; Tsai, M. L.; Ho, S. T.; Tai, S. H.; Ho, C. R.; Tsai, S. H.; Liu, C. W.; Chung, R. J.; He, J. H. Above-11%-Efficiency Organic-Inorganic Hybrid Solar Cells with Omnidirectional Harvesting Characteristics by Employing Hierarchical Photon Trapping Structures. *Nano Lett.* **2013**, *13*, 3658−3663.
(41) Chen, C. Y.; Chen, M. W.; Hsu, C. Y.; Lien, D. H.; Chen, M. J.; He, J. H. Enhanced Recovery Speed of Nanostructured ZnO Photodetectors Using Nanobelt Networks. *IEEE J. Sel. Top. Quantum Electron.* **2012**, *18*, 1807−1811.
(42) Tsai, S. H.; Ho, S. T.; Jhuo, H. J.; Ho, C. R.; Chen, S. A.; He, J. H. Toward High Efficiency of Inverted Organic Solar Cells: Concurrent Improvement in Optical and Electrical Properties of Electron Transport Layers. *Appl. Phys. Lett.* **2013**, *102*, 253111.
(43) Ozone Producing Germiciddal Lamp Spectral Energy Distribution http://www.rexim.com/pages/ccfl/hfuv.html (accessed Sep 23, 2017).
(44) Tsai, D. S.; Lien, D. H.; Tsai, M. L.; Su, S. H.; Chen, K. M.; Ke, J. J.; Yu, Y. C.; Li, L. J.; He, J. H. Trilayered MoS_2 Metal-Semiconductor-Metal Photodetectors: Photogain and Radiation Resistance. *IEEE J. Sel. Top. Quantum Electron.* **2014**, *20*, 3800206.
(45) Wei, T. C.; Tsai, D. S.; Ravadgar, P.; Ke, J. J.; Tsai, M. L.; Lien, D. H.; Huang, C. Y.; Horng, R. H.; He, J. H. See-Through Ga_2O_3 Solar-Blind Photodetectors for Use in Harsh Environments. *IEEE J. Sel. Top. Quantum Electron.* **2014**, *20*, 3802006.

DOI: 10.1021/acsnano.7b04804
ACS Nano 2017, 11, 10230−10235